2020 IEEE/RSJ International Conference on Intelligent Robots and Systems (IROS)
October 25-29, 2020, Las Vegas, NV, USA (Virtual)

2020 IEEE/RSJ International Conference on Intelligent Robots and Systems (IROS) | 978-1-7281-6212-6/20/$31.00 ©2020 IEEE | DOI: 10.1109/IROS45743.2020.9341110

Application of Interacting Models to Estimate the Gait Speed of an Exoskeleton User

Roopak M. Karulkar[1], Patrick M. Wensing[1]

***Abstract*— This paper outlines steps toward a framework for model-based user intent detection to enable fluent human-robot interaction in assistive exoskeletons. An interacting multi-model (IMM) estimation scheme is presented to address state estimation for lower-extremity exoskeletons and to handle their hybrid dynamics. The proposed IMM scheme includes new approaches that enable it to estimate states of hybrid systems with dynamics that are unique to each phase. Traditional IMMs only consider the probabilistic likelihood of being in each phase, while the implementation in this work has been modified to consider physical likelihood as well. The IMM compares exoskeleton sensor readings to multiple candidate gaits from a template model of walking. Candidate gaits are generated using a numerical optimization procedure applied to a Bipedal Spring-Loaded Inverted Pendulum (B-SLIP) model. The framework was tested with sensor data acquired from walking trials in an Ekso GT exoskeleton, and was used to estimate gait phase and center of mass velocity. It is shown that the standard IMM filtering approach results in incorrect estimates of gait phase, while the proposed addition to the IMM estimator using physical likelihood improves the estimates. Results with human subject data further show the ability to estimate gait phase and speed in experimental settings.**

I. Introduction

A. Motivation and Previous Work

The US has 12,000 new cases of Spinal Cord Injury (SCI) each year in addition to the quarter million individuals already living with SCI [1]. The financial burden and the reduction in the quality of life for these individuals increases the importance of rehabilitation. In recent years, robotic exoskeletons have emerged as an effective tool for gait rehabilitation following incomplete SCI. Exoskeletons such as the ReWalk Personal System [2], EksoGT, and Indego [3] have been approved by the FDA for personal and clinical use. These exoskeletons assist the user's joints through desired trajectories and support the user across all phases of the gait cycle. The repeatability and accuracy enabled by the exoskeleton may also help accelerate rehabilitation [4] while providing the user with increased autonomy. Providing this autonomy to the user will require a high level of fluency in the Human Robot Interaction (HRI) to ensure safe and effective operation.

Fluency in HRI depends heavily on accurate user intent detection, which can be separated into model-based and learning-based methods. Learning-based strategies have been applied in both upper- and lower-limb prosthetic and orthotic devices [5], [6], [7]. However, the considerable variability of human gait may make it difficult for these approaches, as training often requires prohibitive amounts of data. Additionally, the learned relationships may need to be retrained periodically as the gait evolves due to changes in physiology, adaptation to HRI [8], and to the presence of different users.

Fig. 1. Ekso GT exoskeleton. This work considers state estimation and gait phase detection for lower-extremity exoskeletons and tests the framework on data from human-subject tests with the Ekso GT.

In contrast to learning-based intent detection strategies, a less common approach is model-based detection, which uses system dynamics and sensor feedback to infer user intent [9]. Model-based intent estimation strategies for lower-extremity devices may use simplified models of locomotion, also called template models. Templates can approximate key features of human gait based on readily available parameters such as leg length and total mass, making them easily adapted to accommodate different users. Commercially available exoskeletons like the ReWalk and Ekso GT currently rely on explicit user input via buttons or joysticks to capture user intent. The goal of this work is, instead, to develop an inference system that does not require explicit user inputs and can be computed using kinematic sensor data alone. There has been some previous work on model-based user intent detection in lower-extremity exoskeletons by modeling the user with the Linear Inverted Pendulum (LIP) to infer intent based on the orbital energy [10]. A method of indirect user-intent inference was presented by Brescanini et al. [11] that infers user intent based on step-to-step crutch positions estimated using crutch-mounted IMUs. However, this approach does not use any representation of the dynamics of legged locomotion, and doing so through template models may make it easier to generalize performance to a wider user base.

Incorporating dynamic models of legged locomotion into intent recognition presents challenges due to their often hybrid nature. Hybrid dynamics arise since each phase of

[1] Authors are with the Department of Aerospace and Mechanical Engineering, University of Notre Dame, Notre Dame, IN, USA. This work was supported by the National Science Foundation under Grant IIS-1734532.

the gait (e.g., single support, double support, etc.) is conventionally described by a different set of dynamics, with transitions between phases subject to switching conditions. The inclusion of these multiple dynamic modes makes the state estimation problem more difficult since state estimation relies on the accurate inference of mode. This issue is remedied herein through the use of Interacting Multi-Model estimators (IMMs). While IMMs have been used for state estimation of hybrid systems (e.g., [12], [13]), their application to legged locomotion has been minimal. A notable example is the use of IMMs for state estimation and the prediction of gait phase in RHex, a six-legged robot with compliant legs [14].

B. Contribution

Accurate state estimation is a foundational component for intuitive user intent detection in HRI, as it would deliver increased insight into user actions. The main contribution of this work is an IMM estimation framework that compares a library of gaits generated from a template model to sensor measurements from an exoskeleton. The library contains walking gaits with speeds up to 1 m/s, and is built using a predictor-corrector type gait search algorithm to address the low dynamic stability of the model at low speeds. The framework is able to estimate the center of mass (CoM) state as the user transitions through the different phases of the gait.

C. Overview

This paper explores the use of gaits generated using template models of human locomotion to estimate the velocity and gait phase of an exoskeleton user from sensor measurements. Since this work considers application for individuals recovering from SCI, the considered walking velocities were as low as 0.4 m/s [15]. Inter-subject and intra-subject variability that exists in human locomotion is further pronounced following SCI due to spasticity [16]. This variability motivates the use of model-based intent detection using simple models of legged locomotion in an effort to capture walking patterns that hold across individuals. Section II details the template model used to describe low-speed walking and outlines optimization methods to find periodic gaits at low speeds. An IMM estimation framework is presented in Section III and is shown to overcome mode selection challenges presented by hybrid dynamics. The results of applying this framework to state estimation with experimental data are presented in Section IV, and concluding remarks are provided in Section V.

II. Gait Library Generation

A. Modeling Human Walking - Bipedal SLIP

Although humans are high degree of freedom systems, many whole-body movements can be accurately abstracted by reduced-order models, often called templates [18]. Template models replicate salient kinematic and kinetic characteristics of the complex neuro-muscular interactions involved in locomotion. The Bipedal Spring-Loaded Inverted Pendulum (B-SLIP) model [19] is an appropriate model for walking due to its ability to capture key gait features such as time spent in double support. In the B-SLIP model, the CoM is loaded onto two massless spring legs of fixed stiffness with rest length l_0.

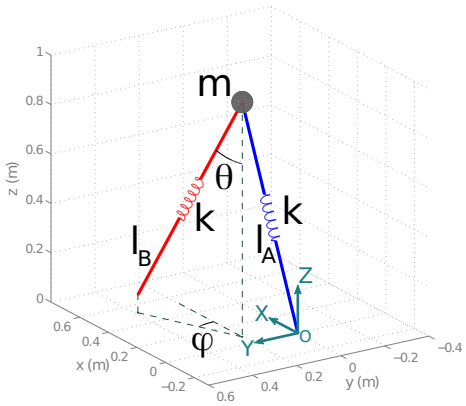

Fig. 2. The Bipedal Spring-Loaded Inverted Pendulum (B-SLIP) model [17] of walking used for state estimation in this work.

A 3D generalization [17] of the 2D model proposed by Geyer [19] is adopted in this work, and is illustrated in Fig. 2. The emphasis on including lateral dynamics from the 3D model is motivated by the low walking speeds considered here, as the peak-to-peak amplitude of lateral CoM excursion is approximately 3 cm while walking at 1.27 m/s but it rises to 9 cm while walking at 0.44 m/s [20]. Gaits for the B-SLIP model can be specified through parameters $\boldsymbol{\xi} = [\phi,\ \theta,\ k,\ z_{0_{\mathrm{CoM}}},\ y_{0_{\mathrm{CoM}}}, \dot{x}_{0_{\mathrm{CoM}}}]$ where ϕ and θ are leg angles that govern step length and step width, k is the leg stiffness, and the variables $z_{0_{\mathrm{CoM}}}$, $y_{0_{\mathrm{CoM}}}$, and $\dot{x}_{0_{\mathrm{CoM}}}$ give the vertical position, lateral position, and forward velocity of the CoM relative to the foot at the beginning of a stride.

B. Gait Optimization Setup

To determine parameters for periodic gaits, an optimization procedure was carried out considering the state evolution over one step. A gait of the B-SLIP model is chosen to start at midstance (MS), where the CoM is loaded onto the trailing leg in single-support (SS1). The gait then proceeds with the touchdown (TD) of the leading leg and enters the double support (DS) phase. The DS phase ends with lift-off (LO) of the trailing leg and the model enters the second single-support phase (SS2). The SS2 phase ends in MS, again with the CoM loaded onto the leading leg. Gait optimization was considered via a nonlinear programming problem

$$\min_{\boldsymbol{\xi}} \quad \|\boldsymbol{J}(\boldsymbol{\xi})\|^2 + (k_{max} - k) \tag{1}$$

$$\text{s.t.} \quad \boldsymbol{g}(\boldsymbol{\xi}) \leq \epsilon \tag{2}$$

where $\boldsymbol{J}(\boldsymbol{\xi})$ is a vector-valued function returning the vertical excursion of the CoM, deviation from a desired step length and width, and the distance from the ground projection of the CoM to the foot at MS. Nonlinear constraint functions $\boldsymbol{g}(\boldsymbol{\xi})$ ensure periodicity of the gait by matching the initial and final positions and velocities of the CoM with respect to the trailing foot.

Initially, the trajectories of optimized periodic gaits exhibited lower lateral excursion and higher vertical excursion for

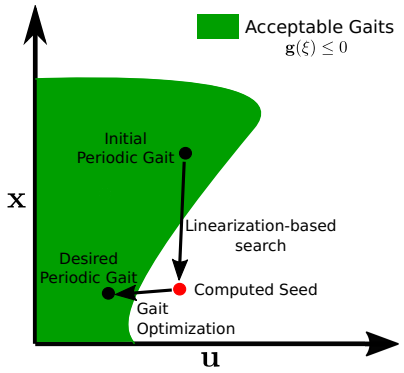

Fig. 3. Depiction of the linearization-based predictor-corrector search scheme to find periodic low-speed gaits.

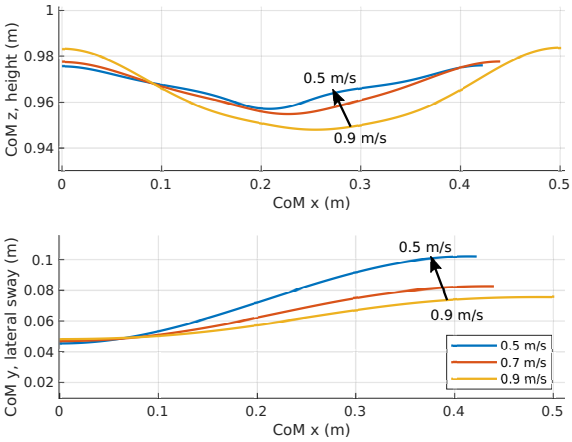

Fig. 4. A subset of the CoM trajectories in the gait library after optimization.

the CoM than observed in human data. This behavior was remedied by driving leg stiffness toward an upper limit with 1) the inclusion of $(k_{max} - k)$ in the cost, and 2) penalizing the maximum vertical excursion of the CoM through its inclusion in $\boldsymbol{J}(\boldsymbol{\xi})$. Additionally, constraints on the step length and width were found to be critical for the convergence of the optimization. Desired step length and width were approximated as a function of speed [21] using a polynomial fit to human walking data [20]. As speed decreases, it is progressively difficult to choose appropriate parameters to seed the optimization, as the sensitivity of the model to initial conditions increases due to low passive stability at low speeds [22]. A linearization-based predictor-corrector scheme was applied to start at a high-speed gait and compute appropriate seeds for low-speed gaits.

C. Linearization-Based Seed Search

Empirically, gaits at speeds greater than 0.8 m/s were directly found through optimization of (1) without special attention to initial seeds. To address challenges for lower target velocities, a predictor-corrector type strategy (Fig. 3) was applied. The strategy used a linearized Poincaré return map to solve for a preliminary seed during a homotopy process toward a lower-speed gait. As part of the process, the step-to-step dynamics are described by a Poincaré return map

$$\mathbf{x}_{k+1} = \mathcal{P}(\mathbf{x}_k, \mathbf{u}_k) \tag{3}$$

where $\mathbf{x}_k$ denotes the state at MS and $\mathbf{u}_k$ denotes the discrete controls applied over one step as given by

$$\mathbf{x} = [y_{\text{CoM}},\ z_{\text{CoM}},\ \dot{x}_{\text{CoM}},\ \dot{y}_{\text{CoM}}]^T \quad \mathbf{u} = [\phi,\ \theta,\ k]^T \tag{4}$$

The vertical velocity satisfies $\dot{z} = 0$ at MS, and thus $\dot{z}$ is omitted from the state $\mathbf{x}_k$ on the Poincaré surface. Following the optimization of one step of a periodic gait with state and control $\mathbf{x}_k^*$, $\mathbf{u}_k^*$, the return map is linearized providing

$$\mathbf{x}_{k+1} \approx \mathbf{x}_{k+1}^* + \underbrace{\left.\frac{\partial \mathcal{P}}{\partial \mathbf{x}}\right|_{\mathbf{x}_k^*, \mathbf{u}_k^*}}_{:=\mathbf{A}} \delta\mathbf{x}_k + \underbrace{\left.\frac{\partial \mathcal{P}}{\partial \mathbf{u}}\right|_{\mathbf{x}_k^*, \mathbf{u}_k^*}}_{:=\mathbf{B}} \delta\mathbf{u}_k \tag{5}$$

where $\mathbf{x}_{k+1}^* = \mathcal{P}(\mathbf{x}_k^*, \mathbf{u}_k^*)$, $\delta\mathbf{x}_k = \mathbf{x}_k - \mathbf{x}_k^*$, and $\delta\mathbf{u}_k = \mathbf{u}_k - \mathbf{u}_k^*$. Since a gait of the 3D B-SLIP model is two-step periodic, left/right symmetry from step to step requires that $\mathbf{x}_{k+1}^* = \mathbf{S}\mathbf{x}_k^*$ where $\mathbf{S} = \text{diag}([-1, 1, 1, 1])$. This matrix encodes that only the y-position of the CoM relative to the foot must change signs from step to step. Then, to solve for an approximate state/control pair for a lower-speed gait, variations to the parameters were found such that $\delta\mathbf{x}_{k+1} = \mathbf{S}\delta\mathbf{x}_k$. This constraint requires

$$\mathbf{0} = (\mathbf{A} - \mathbf{S})\delta\mathbf{x}_k + \mathbf{B}\delta\mathbf{u}_k\,. \tag{6}$$

To generate a suitable next seed, the forward velocity component of $\delta\mathbf{x}_k$ was held constant to the desired change in velocity. Considering (6), these equations provide 4 constraints for the 6 remaining unknowns, $[\delta y_{\text{CoM}},\ \delta z_{\text{CoM}},\ \delta \dot{y}_{\text{CoM}},\ \delta\phi,\ \delta\theta,\ \delta k]^T$, resulting in 2 degrees of freedom. Perturbations $\delta\mathbf{x}_k$ and $\delta\mathbf{u}_k$ satisfying these equations were computed with a least-norm solution, and the resulting parameters were used to seed the next gait optimization. This homotopy process was repeated until the desired low-velocity gait was optimized, resulting in a library of gaits for a range of speeds. Two libraries were generated: one at 0.4 m/s - 0.9 m/s for use with B-SLIP data and another at 0.6 m/s - 1.0 m/s for use with exoskeleton measurements, both at increments of 0.1 m/s. As illustrated in Fig. 4, generated libraries qualitatively exhibit the vertical and lateral CoM excursion trends that are observed in human data. That is, vertical excursion decreases and lateral excursion increases with a decrease in forward velocity. This linearization-based gait search method makes the generation of low-speed gaits easier and yields a library that serves as the basis for the IMM outlined in the next section.

III. Multi-Model Estimation

Legged locomotion is described using hybrid dynamics that switch based on gait events of touchdown and lift-off. IMMs handle state estimation for these hybrid dynamics by assigning each mode of the B-SLIP gait as a separate model in the estimation framework. This approach results in $M = N \times m$ estimators being run in parallel, where N is the

TABLE I

CONTINUOUS-DISCRETE EXTENDED KALMAN FILTER

Model	$\dot{\mathbf{x}}(t) = \mathbf{f}(\mathbf{x}(t), \mathbf{u}(t), \mathbf{w}(t), t), \quad \mathbf{w}(t) \sim \mathcal{N}(0, \mathbf{Q}(t))$ $\tilde{\mathbf{y}}_k = \mathbf{h}(\mathbf{x}_k) + \mathbf{v}_k, \quad \mathbf{v}_k \sim \mathcal{N}(0, \mathbf{R}_k)$
Propagation	$\dot{\hat{\mathbf{x}}}(t) = \mathbf{f}(\hat{\mathbf{x}}(t), \mathbf{u}(t), 0, t)$ $\dot{\mathbf{P}}(t) = \mathbf{F}(t)\mathbf{P}(t) + \mathbf{P}(t)\mathbf{F}^T(t) + \mathbf{G}(t)\mathbf{Q}(t)\mathbf{G}(t)^T$ $\mathbf{F}(t) \equiv \frac{\partial \mathbf{f}}{\partial \mathbf{x}}\Big\vert_{\hat{\mathbf{x}}(t),\mathbf{u}(t)} \quad \mathbf{G}(t) \equiv \frac{\partial \mathbf{f}}{\partial \mathbf{w}}\Big\vert_{\hat{\mathbf{x}}(t),\mathbf{u}(t)}$
Gain	$\mathbf{K}_k = \mathbf{P}_k^- \mathbf{H}_k^T(\hat{\mathbf{x}}_k^-) \left[\mathbf{H}_k(\hat{\mathbf{x}}_k^-)\mathbf{P}_k^- \mathbf{H}_k^T(\hat{\mathbf{x}}_k^-) + \mathbf{R}_k\right]^{-1}$
Update	$\hat{\mathbf{x}}_k^+ = \hat{\mathbf{x}}_k^- + \mathbf{K}_k[\tilde{\mathbf{y}}_k - \mathbf{h}(\hat{\mathbf{x}}_k^-)]$ $\mathbf{P}_k^+ = [\mathbf{I} - \mathbf{K}_k\mathbf{H}_k(\hat{\mathbf{x}}_k^-)]\mathbf{P}_k^-, \quad \mathbf{H}_k(\hat{\mathbf{x}}_k^-) \equiv \frac{\partial \mathbf{h}}{\partial \mathbf{x}}\Big\vert_{\hat{\mathbf{x}}_k^-}$

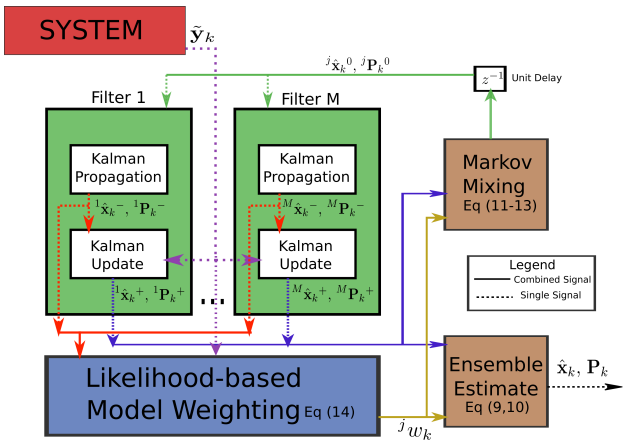

Fig. 5. IMM scheme used to estimate gait phase and walking speed.

number of gaits in the library and $m = 3$ is the number of hybrid modes (SS1, DS, SS2) for each gait. As detailed in this section, the individual estimators are chosen as Extended Kalman filters, with the outputs of these parallel filters then fused with a likelihood-based weighted average to produce an ensemble state estimate.

A. Extended Kalman Filtering

The building block of the IMM estimation scheme is the Extended Kalman filter (EKF). Each filter starts at some initial state, that state estimate is propagated forward in time, and the estimate is corrected using sensor feedback. This work considers continuous-time dynamics and discrete-time measurements, with the resulting EKF equations given in Table I. In this table, and in what follows, $\mathbf{x}(t)$ and $\mathbf{u}(t)$ are the continuous-time states and inputs, $\mathbf{y}_k$ are the discrete-time measurements, and $\mathbf{f}(\mathbf{x}(t), \mathbf{u}(t), \mathbf{w}(t), t)$ and $\mathbf{h}(\mathbf{x}_k)$ are the system dynamics and measurement function respectively. The system is assumed to have zero-mean Gaussian process and measurement noises $\mathbf{w}(t)$ and $\mathbf{v}_k$ with covariances $\mathbf{Q}(t)$ and $\mathbf{R}_k$ respectively. The vector $\mathbf{v}_k$ contributes to a noisy measurement denoted by $\tilde{\mathbf{y}}_k = \mathbf{h}(\mathbf{x}_k) + \mathbf{v}_k$ that is used in the Kalman update. Throughout, superscripts $-$ and $+$ denote estimates before and after considering this measurement.

B. Interacting Multi-Model Filtering (IMM)

The IMM adaptively fuses the estimates from multiple filters through the process illustrated in Fig. 5. Each of the M filters represents a different candidate gait and mode, and the IMM attempts to determine which of the modes is most likely. In what follows, i and j index over filters, and k indexes over time. There are two types of estimate interactions shown in Fig. 5. A likelihood-based mixing produces an ensemble estimate output from the IMM, while a Markov mixing relates the state estimates from the filters at time step k to the initial estimates at time step $k+1$.

The filters begin with initial state estimates $^j\hat{\mathbf{x}}_k^0$ and covariances $^j\mathbf{P}_k^0$ that are propagated forward to $^j\hat{\mathbf{x}}_k^-$ and $^j\mathbf{P}_k^-$ using the dynamics presented in Table I. The measurement likelihood $^j\ell_k$ is then calculated for the state estimate of each filter as

$$^j\ell_k = p(\tilde{\mathbf{y}}_k \vert\, ^j\hat{\mathbf{x}}_k^-) = \det(2\pi\, ^j\mathbf{E}_k)^{-1/2}\, e^{\lambda_r} \quad \text{where} \tag{7}$$

$$\lambda_r = -\frac{1}{2}\, ^j\mathbf{e}_k^T\, ^j\mathbf{E}_k^{-1}\, ^j\mathbf{e}_k$$

and $^j\mathbf{e}_k$ and $^j\mathbf{E}_k$ denote the measurement residual and its covariance, respectively, given by $^j\mathbf{e}_k = \tilde{\mathbf{y}}_k - \mathbf{h}\left(^j\hat{\mathbf{x}}_k^-\right)$ and

$$^j\mathbf{E}_k = {}^j\mathbf{H}_k\ {}^j\mathbf{P}_k^-\ {}^j\mathbf{H}_k^T + {}^j\mathbf{R}_k.$$

with $^j\mathbf{H}_k$ the Jacobian of the measurement function at $^j\hat{\mathbf{x}}_k^-$.

The measurement likelihood is then normalized across the M models to calculate model weights ^jw_k via

$$^jw_k = {}^j\ell_k \Big/ \left(\textstyle\sum_{i=1}^M {}^i\ell_k\right) \tag{8}$$

The magnitude of the weight ^jw_k indicates the relative confidence of the filter that the system is in mode j at time step k. In contrast to a conventional IMM approach [23] where $^jw_k = {}^jw_{k-1} p(\tilde{\mathbf{y}}_k \vert\, ^j\hat{\mathbf{x}}_k^-)$, the weights from the previous iteration are not included in (8). This change was due to the fact that some likelihoods, e.g., likelihoods for DS models during SS, result in numerically zero weights, from which it is not possible to recover to non-zero weights.

Following the computation of the likelihood for each model, the noisy measurement $\tilde{\mathbf{y}}_k$ is used with the Kalman update in Table I to produce a posteriori estimates $^j\mathbf{x}_k^+$ and covariances $^j\mathbf{P}_k^+$. These quantities are fused to produce an ensemble estimate $\hat{\mathbf{x}}_k$ with covariance $\mathbf{P}_k$ calculated via

$$\hat{\mathbf{x}}_k = \textstyle\sum_{j=1}^M {}^jw_k\, {}^j\hat{\mathbf{x}}_k^+ \tag{9}$$

$$\mathbf{P}_k = \sum_{j=1}^M {}^jw_k \left[\left({}^j\hat{\mathbf{x}}_k^+ - \hat{\mathbf{x}}_k\right)\left({}^j\hat{\mathbf{x}}_k^+ - \hat{\mathbf{x}}_k\right)^T + {}^j\mathbf{P}_k^+\right] \tag{10}$$

Fusion from (10) captures the covariance of each individual filter and of each filter estimate with the fused estimate.

Initial conditions for the next time step $^j\hat{\mathbf{x}}_{k+1}^0$ are then computed considering interaction between the models as

$$^j\hat{\mathbf{x}}_{k+1}^0 = \textstyle\sum_{i=1}^M {}^{(i|j)}w_k\, {}^i\hat{\mathbf{x}}_k^+ \tag{11}$$

where $^{(i|j)}w_k$ is a weight that considers a likelihood-based model probability and a Markov-based transition probability from model i to model j. Markov transition probabilities p_{ij}

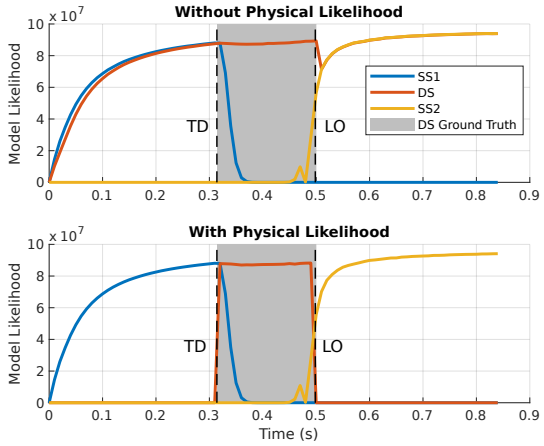

Fig. 6. The effects of the inclusion of physical likelihood on phase likelihoods

are specified as fixed probabilities of switching from i to j and

$$ {}^{(i|j)}w_k = {}^{i}w_k p_{ij} / \left(\sum_{s=1}^{M} {}^{s}w_k p_{sj} \right) \tag{12} $$

Similarly, a mixed covariance for the next iteration is computed through

$$ {}^{j}\mathbf{P}_{k+1}^{0} = \sum_{i=1}^{M} {}^{(i|j)}w_k \left[{}^{(i|j)}\mathbf{e}_k \, {}^{(i|j)}\mathbf{e}_k^T + {}^{i}\mathbf{P}_k^{+} \right] , \text{ where} \tag{13} $$

$$ {}^{(i|j)}\mathbf{e}_k = {}^{i}\hat{\mathbf{x}}_k^{+} - {}^{j}\hat{\mathbf{x}}_{k+1}^{0} $$

A small modification to the conventional IMM was necessary to enable the framework to correctly identify gait modes. The likelihood calculation (7) only looks at the measurement residual, which can be misleading. Dynamics during DS can track the CoM trajectories from SS data by allowing legs to extend beyond their free length, which is not physically possible. A physical likelihood term λ_p was added to the likelihood calculation to address this observation. This strategy takes into account the difference Δl between the rest length and current length of the leg, which should remain positive. The likelihood is then modified as

$$ {}^{j}\ell_k = \det(2\pi \, {}^{j}\mathbf{E}_k)^{-1/2} \, e^{\lambda_r + \lambda_p} , \text{ where} \tag{14} $$

$$ \lambda_p = -\kappa \min(0, \Delta l)^2 $$

and $\kappa > 0$ is a tuning parameter. In DS, the leg with the minimum value for Δl is used to compute λ_p. This approach decreases the weight of a model if its estimated leg length is greater than its rest length. Figure 6 shows the effect this modification has on phase inference. With the change, the likelihood of DS only rises during the true DS phase, illustrated with the shaded area. The rate at which the likelihood of DS rises and decays can be tuned using κ.

IV. Results & Discussion

A. Testing with B-SLIP Simulation Data

The framework was initially tested on data generated using the B-SLIP model. The gait used to generate measurements was a gait from the library with forward velocity $\dot{x}_{\text{CoM}} = 0.7$ m/s. Measurements of 3D position and sagittal plane velocity of the CoM were used such that $\mathbf{y} = [x_{\text{CoM}}, \, y_{\text{CoM}}, \, z_{\text{CoM}}, \, \dot{x}_{\text{CoM}}, \, \dot{z}_{\text{CoM}}]^T$. Zero-mean Gaussian noise with constant covariance $\mathbf{R}$ was added to the simulated measurements. Process noise was not added to the simulation. During estimation, inaccuracies in the dynamics exist when an inaccurate mode/gait is used, therefore the process noise covariance $\mathbf{Q}$ was retained as a tuning parameter for the estimation. The covariance values used are given by

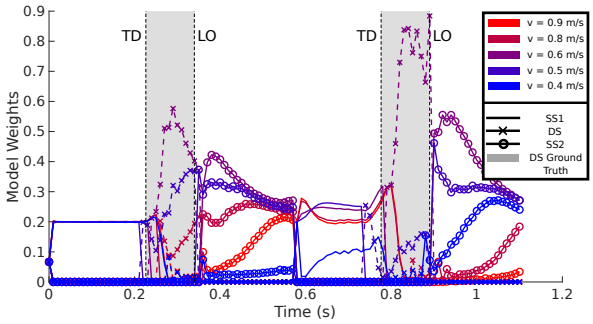

Fig. 7. Model weights output by the IMM framework applied to measurements generated from a simulation of the B-SLIP model.

$$ \mathbf{R} = \text{diag}([5, 5, 5, 50, 50]) \times 10^{-5} \tag{15} $$

$$ \mathbf{Q} = \text{diag}([0, 0, 0, 1, 1, 1]) \times 10^{-2} \tag{16} $$

where continuous process noise variances for positions and velocities are reported with units m^2/s^2 and m^2/s^4 respectively, and discrete measurement variances for positions and velocities are reported with units m^2 and m^2/s^2 respectively.

The gait used for generating measurements was then excluded from the estimation library for testing. Fig. 7 shows the weights associated with each model over two gait cycles of estimation. Since a gait that exactly matches the measurements is not available in the library, the framework estimates the gait at $\dot{x}_{\text{CoM}} = 0.6$ m/s to be the most likely. The framework has difficulty distinguishing gaits in the beginning due to their similarity in SS1. The differences in gait trajectories becomes more apparent as the gait progresses through DS. This behavior is explained by the effectiveness of the B-SLIP model for capturing the dynamics of DS (e.g., compared to traditional rigid pendular models that assume an instantaneous transfer of support). The differences between gaits in the next SS1 phase are more pronounced and the framework displays more confidence in the most likely gait.

B. Testing with Exoskeleton Experiment Data

The algorithm was then tested on data acquired from the sensors on board a robotic exoskeleton (Ekso GT) during the walking trials of an able-bodied person. The subject had a leg length of 0.95 m, weighed 67 kg, and walked at a self-selected speed between 0.6 - 0.7 m/s with the aid of crutches [24]. The exoskeleton allows movement only in the sagittal plane and restricts movements in the lateral direction, however, some lateral movement of the CoM is observed due to torso roll. Consequently, the measurements

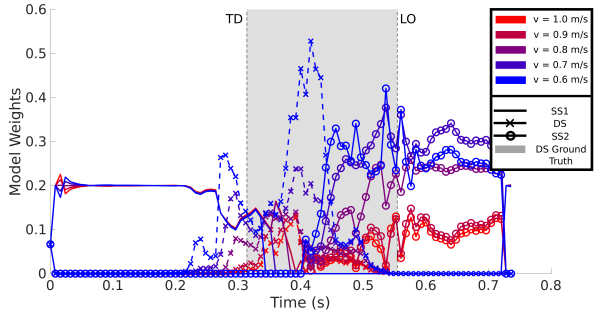

Fig. 8. Model weights from the IMM framework applied to experimental measurements of an able-bodied individual walking in an exoskeleton.

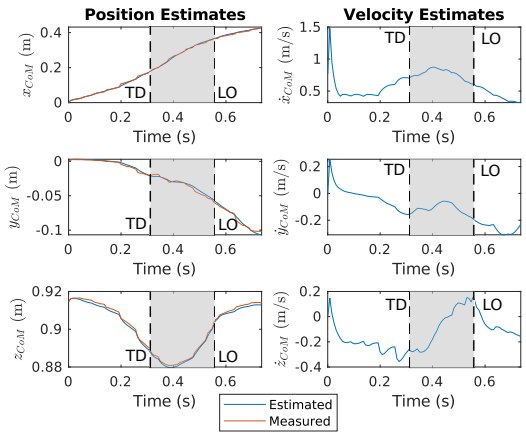

Fig. 9. State estimates from the IMM framework applied to experimental measurements of an able-bodied individual walking in an exoskeleton.

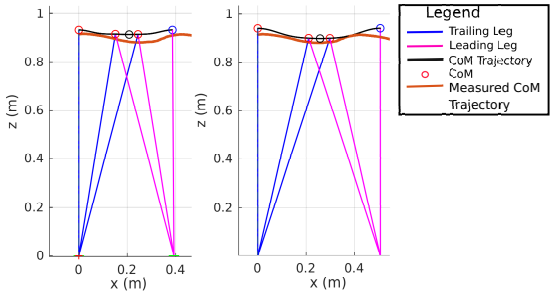

Fig. 10. Comparison of gaits at speeds of 0.6 m/s (left) and 1.0 m/s (right).

available for use were the forward and vertical position of the left and right side of the hips and the torso roll angle obtained from an Inertial Measurement Unit (IMU) mounted on the exoskeleton. The position of the CoM in 3D was approximated using these measurements, with the measurement vector given by $\tilde{\mathbf{y}} = [x_{\text{CoM}},\ y_{\text{CoM}},\ z_{\text{CoM}}]^T$. The B-SLIP CoM evolution is sensitive to changes in the leg length of library gaits, with sensitivity predominantly in the vertical direction. From this motivation, anisotropic process and measurement noise covariances were selected as follows.

$$\mathbf{R} = \text{diag}([5, 5, 0.5]) \times 10^{-6} \tag{17}$$

$$\mathbf{Q} = \text{diag}([0, 0, 0, 1, 1, 10]) \times 10^{-2} \tag{18}$$

This anisotropic covariance selection mitigates sensitivity by decreasing emphasis on the model and increasing the reliance on the measurements when inferring vertical CoM evolution. This strategy was found to yield more accurate velocity estimates in comparison to an isotropic covariance selection. To further mitigate sensitivity due to the leg length parameter, gaits in the library were rescaled based on the measured CoM height at MS. The most likely gaits as determined by the framework are seen in Fig. 8; higher weights indicate a more likely gait.

All gaits in the library have features matching human data, i.e., maximum forward velocity is achieved during double support, and the lateral velocity returns to zero at the end of the step. Yet, the initial height and lateral position of the CoM were variables while optimizing the gait library, and as a result, they don't match exactly with the initial position in the measured data. Therefore, states without direct measurement (all velocities) take ≈50 ms to stabilize to expected behavior, as illustrated in Fig. 9 where estimates are plotted along with measured values. The DS period noted was determined by when foot-mounted force sensors on the exoskeleton indicated that both feet were flat on the ground.

The exoskeleton user was walking at a velocity between 0.6 m/s and 0.7 m/s, however, the sagittal plane evolution of the CoM matches more closely to the library gait at a speed of 1.0 m/s, as illustrated in Fig. 10. This behavior may be due to the dynamics of walking in an exoskeleton with an ambulatory device. The differences in the trajectories become increasingly clear as the gait progresses. Despite this discrepancy between the trajectories, the IMM framework is able to identify the correct velocity with measured data and identifies the correct phase over the majority of the gait. Since the library contains gaits with forward velocities of 0.6 m/s and 0.7, and the measured CoM evolution was between these two velocities, the IMM framework consistently chooses those two gaits as most likely as seen in Fig. 8. Thus, the IMM framework functions as expected, but it relies on an accurate gait library for accurate estimation.

C. Discussion

It can be seen in Fig. 7 and Fig. 8 that there is an inaccuracy in the likelihoods of some phases around phase transitions. This behavior is an artifact of the variety of the gait library. Realistic likelihood calculation is dependent on leg length computation for the physical likelihood. As step length is dependent on velocity, the step length of gaits in the library varies considerably (≈4 cm). For example, even with the leg length rescaling, this discrepancy between the library and the human data causes the likelihood function to detect double support and infer the end of single support at different times, which causes differences in likelihood switching times. However, the combined state estimates on the CoM positions are still accurate to within 1 cm of the measurements (Fig. 9).

Gait phase estimation is possible by directly using force sensors in the exoskeleton soles [25], [26]. However, by relating human data to template models, the presented approach may provide insight into unmeasured parameters, such as

leg stiffness, and the effects of changes in them on the gait. In contrast to using template models, gait phase estimation can be done using data-driven modeling [27], which is more suited for personalized assistance. Due to the generalized nature of template models, the IMM-based approach may apply to a broader set of exoskeleton users.

There are still are discrepancies between the trajectories in the library and human gait, and these discrepancies could be reduced in future work through further refinement of the library or refinement of the template model. One way to improve the library would be to nondimensionalize its gaits so that they can be reparameterized to suit new users with minimal rework. The potential need for modifications to the template is motivated by the additional accuracy required of them in state estimation as compared to previously. The B-SLIP model was historically motivated by the fact that it qualitatively displays the characteristic M-shaped ground reaction force profile of human walking. The use of such models for accurate state estimation requires quantitative accuracy beyond these previous qualitative considerations. One key area for modifications, for example, would be to address the effects of assistive devices (walkers or crutches) that were required with the exoskeleton in this study.

V. Conclusion & Future Work

In conclusion, the IMM framework is capable of determining the correct phase of the gait that most closely matches measurements during state estimation with a lower-extremity exoskeleton. However, it is shown that the quality of the estimates and the performance of the IMM are highly dependent on the quality of the gait library used. The measured CoM trajectories are observed to be asymmetric, and often do not offer a high fidelity match to the trajectories of gaits in the library. The effect of ambulatory devices on walking dynamics may need to be incorporated in a revised gait generation scheme or the Kalman filter formulation may require amendments to accommodate the gait asymmetry and the errors resulting from it. These future changes would increase the estimation accuracy of the framework, paving the way for its use in user intent detection.

References

[1] "Spinal cord injury: Hope through research." [Online]. Available: https://www.ninds.nih.gov/Disorders/Patient-Caregiver-Education/Hope-Through-Research/Spinal-Cord-Injury-Hope-Through-Research

[2] "Rewalk personal exoskeleton system cleared by FDA for home use," https://rewalk.com/rewalk-robotics-announces-expansion-to-india-with-saimed-innovations-2-2-2-2-3-2-3/.

[3] F. Sup, A. Bohara, and M. Goldfarb, "Design and control of a powered transfemoral prosthesis," *The International Journal of Robotics Research*, vol. 27, no. 2, pp. 263–273, 2008.

[4] J. Hidler and R. Sainburg, "Role of robotics in neurorehabilitation," *Topics in Spinal Cord Injury Rehabilitation*, vol. 17, no. 1, pp. 42–49, 2011.

[5] H. Huang, F. Zhang, L. J. Hargrove, Z. Dou, D. R. Rogers, and K. B. Englehart, "Continuous locomotion-mode identification for prosthetic legs based on neuromuscular–mechanical fusion," *IEEE Transactions on Biomedical Engineering*, vol. 58, no. 10, pp. 2867–2875, 2011.

[6] J. Jung, I. Jang, R. Riener, and H. Park, "Walking intent detection algorithm for paraplegic patients using a robotic exoskeleton walking assistant with crutches," *International Journal of Control, Automation and Systems*, vol. 10, no. 5, pp. 954–962, 2012.

[7] T. Gambon, J. P. Schmiedeler, and P. M. Wensing, "Exoskeleton user intent identification via the mahalanobis distance," in *IEEE RAS/EMBS International Conference on Biomedical Robotics and Biomechatronics (to appear)*, 2020.

[8] D. Kulic and E. A. Croft, "Affective state estimation for human-robot interaction," *IEEE Transactions on Robotics*, vol. 23, no. 5, pp. 991–1000, 2007.

[9] J. P. Schmiedeler and P. M. Wensing, "Discussion of "A Review of Intent Detection, Arbitration, and Communication Aspects of Shared Control for Physical Human–Robot Interaction" (Losey, D. P., McDonald, C. G., Battaglia, E., and O'Malley, M. K., 2018, ASME Appl. Mech. Rev., 70(1), p. 010804)," *Applied Mechanics Reviews*, vol. 70, no. 1, 2018.

[10] Q. Chen, H. Cheng, C. Yue, R. Huang, and H. Guo, "Dynamic balance gait for walking assistance exoskeleton," *Applied Bionics and Biomechanics*, vol. 2018, 2018.

[11] D. Brescianini, J.-Y. Jung, I.-H. Jang, H. S. Park, and R. Riener, "INS/EKF-based stride length, height and direction intent detection for walking assistance robots," in *IEEE International Conference on Rehabilitation Robotics*, 2011, pp. 1–5.

[12] Y. Bar-Shalom, S. Challa, and H. A. Blom, "IMM estimator versus optimal estimator for hybrid systems," *IEEE Transactions on Aerospace and Electronic Systems*, vol. 41, no. 3, pp. 986–991, 2005.

[13] E. Daeipour and Y. Bar-Shalom, "IMM tracking of maneuvering targets in the presence of glint," *IEEE Transactions on Aerospace and Electronic Systems*, vol. 34, no. 3, pp. 996–1003, 1998.

[14] S. Skaff, A. A. Rizzi, H. Choset, and P.-C. Lin, "A context-based state estimation technique for hybrid systems," in *IEEE International Conference on Robotics and Automation*, 2005, pp. 3924–3929.

[15] J. R. Nymark, S. J. Balmer, E. H. Melis, E. D. Lemaire, and S. Millar, "Electromyographic and kinematic nondisabled gait differences at extremely slow overground and treadmill walking speeds." *Journal of Rehabilitation Research & Development*, vol. 42, no. 4, 2005.

[16] P. Krawetz and P. Nance, "Gait analysis of spinal cord injured subjects: effects of injury level and spasticity," *Archives of Physical Medicine and Rehabilitation*, vol. 77, no. 7, pp. 635–638, 1996.

[17] Y. Liu, P. M. Wensing, D. E. Orin, and Y. F. Zheng, "Dynamic walking in a humanoid robot based on a 3D actuated Dual-SLIP model," in *IEEE International Conference on Robotics and Automation*, 2015, pp. 5710–5717.

[18] R. J. Full and D. E. Koditschek, "Templates and anchors: neuromechanical hypotheses of legged locomotion on land," *Journal of Experimental Biology*, vol. 202, no. 23, pp. 3325–3332, 1999.

[19] H. Geyer, A. Seyfarth, and R. Blickhan, "Compliant leg behaviour explains basic dynamics of walking and running," *Proceedings of the Royal Society B: Biological Sciences*, vol. 273, no. 1603, pp. 2861–2867, 2006.

[20] C. A. Fukuchi, R. K. Fukuchi, and M. Duarte, "A public dataset of overground and treadmill walking kinematics and kinetics in healthy individuals," *PeerJ*, vol. 6, p. e4640, 2018.

[21] T. Andriacchi, J. Ogle, and J. Galante, "Walking speed as a basis for normal and abnormal gait measurements," *Journal of Biomechanics*, vol. 10, no. 4, pp. 261–268, 1977.

[22] A. D. Kuo, "A simple model of bipedal walking predicts the preferred speed–step length relationship," *Journal of Biomechanical Engineering*, vol. 123, no. 3, pp. 264–269, 2001.

[23] J. L. Crassidis and J. L. Junkins, *Optimal Estimation of Dynamic Systems, Second Edition (Chapman & Hall/CRC Applied Mathematics & Nonlinear Science)*, 2nd ed. Chapman & Hall/CRC, 2011.

[24] T. M. Gambon, J. P. Schmiedeler, and P. M. Wensing, "Characterizing intent changes in exoskeleton-assisted walking through onboard sensors," in *IEEE International Conference on Rehabilitation Robotics*, 2019, pp. 471–476.

[25] V. Agostini, G. Balestra, and M. Knaflitz, "Segmentation and classification of gait cycles," *IEEE Transactions on Neural Systems and Rehabilitation Engineering*, vol. 22, no. 5, pp. 946–952, 2013.

[26] S. M. De Rossi, S. Crea, M. Donati, P. Rebersek, D. Novak, N. Vitiello, T. Lenzi, J. Podobnik, M. Munih, and M. C. Carrozza, "Gait segmentation using bipedal foot pressure patterns," in *IEEE RAS/EMBS International Conference on Biomedical Robotics and Biomechatronics*, 2012, pp. 361–366.

[27] A. Kalinowska, T. A. Berrueta, A. Zoss, and T. Murphey, "Data-driven gait segmentation for walking assistance in a lower-limb assistive device," in *IEEE International Conference on Robotics and Automation*, 2019, pp. 1390–1396.